Efficient MIMO Equalization for Downlink Multi-Code CDMA: Complexity Optimization and Comparative Study

Yuanbin Guo, Jianzhong Zhang, Dennis McCain
Nokia Research Center
6000 Connection Drive, Irving, TX, USA, 75039
{Yuanbin.Guo, Charlie.Zhang,
Dennis.McCain}@nokia.com

Joseph R. Cavallaro
Rice University
6100 Main Street, Houston, TX, USA, 77005
cavallar@rice.edu

***Abstract*—In this paper, we present an efficient LMMSE chip equalizer to suppress the interference caused by the multipath fading channel in the MIMO Multi-Code CDMA downlink. The block-Toeplitz structure in the correlation matrix is approximated with a block circulant matrix. An FFT-based algorithm is applied to avoid the Direct-Matrix-Inverse (DMI) in the system equation. *Hermitian* optimization is proposed to further reduce the complexity. A comparative study in both performance and complexity with the Conjugate-Gradient (CG) algorithm is then presented. The simulation shows very promising results for the FFT-based equalizer compared with both the DMI and CG algorithms.**

I. INTRODUCTION

The growing demands for broadband multimedia services, ubiquitous networking via mobile devices push the development of advanced modem technology for much higher data rate than the current 3rd generation cellular systems. UMTS and CDMA2000 extensions optimized for data services lead to the standardization of Multi-Code CDMA systems such as the High-Speed-Downlink-Packet-Access (HSDPA) and its equivalent 1X EV-DV (Evolution Data and Voice) [1][2]. The high data rate is achieved by the assignment of multiple code channels to a single subscriber, shorter spreading gain and high-order modulation schemes. MIMO (Multiple Input Multiple Output) technology [2][3] using multiple antennas at both the transmitter and receiver sides has recently emerged as one of the most significant technical breakthroughs in modern communications. The original invention is known as D-BLAST [2] and a more realistic strategy is V-BLAST [3][4] by nulling and canceling with reasonable tradeoff between complexity and performance. MIMO extensions for the 3G wireless systems have received more and more attention from the research community because of the ability to provide very high spectral efficiency. A working group within 3GPP is currently proposing a MIMO-HSDPA standard.

The original MIMO spatial multiplexing was proposed for narrow band and flat-fading channels. In a multipath-fading channel, the orthogonality of the spreading codes is destroyed and the Multiple-Access-Interference (MAI) along with the Inter-Symbol-Interference (ISI) is introduced. With a very short spreading gain, the conventional Rake receiver could not provide acceptable performance. The LMMSE (Linear-Minimum-Mean-Square-Error)-based chip equalizer is promising to restore the orthogonality of the spreading code, so as to suppress both the ISI and MAI [5].

However, the LMMSE equalizers involve the inverse of a large correlation matrix with the general complexity of $O((NF)^3)$, where N is the number of Rx antenna and F is the channel length. This is very expensive for hardware implementation. The complexity of a MIMO receiver increases dramatically with the number of antennas and the constellation order. The fact that the receiver must be embedded into a portable device makes the design of low complexity mobile receivers very critical for widespread commercial deployment of low cost products. To avoid the Direct-Matrix-Inverse (DMI), adaptive stochastic gradient algorithms such as LMS could be applied [5]. However, they suffer from stability problems because the convergence depends on the choice of good step size. In [6][7], a Conjugate Gradient algorithm is proposed for iterative computation with promising performance.

Because the correlation matrix assumes a block-Toeplitz structure, an FFT-based approximation of the circulant matrix is proposed for SIMO systems in [1][8]. In this paper, we apply the efficient FFT-based algorithm to the MIMO Multi-Code CDMA downlink, which results in complexity on the order of several FFT operations. To further reduce the complexity, *Hermitian* optimization is proposed by utilizing the structures of the correlation coefficients and the FFT algorithm. A reduced-state FFT module is proposed to avoid duplicate computation of the symmetric coefficients and the zero coefficients. A comparative study in both performance and complexity is presented between the Conjugate Gradient and the FFT-based equalizer in compliance with the HSDPA standard for MIMO scenarios. The simulation shows very promising results for the FFT-based equalizer with reduced complexity compared with both the DMI and CG algorithms.

II. SYSTEM MODEL

The system model of the MIMO Multi-Code CDMA downlink using spatial multiplexing is described in Fig. 1. M Tx antennas and N Rx antennas are applied in the system, where usually $M \le N$. In a Multi-Code CDMA system such as HSDPA, multiple spreading codes are assigned to a single user to achieve high data rate. First, the high data rate symbols are demultiplexed into $K*M$ lower rate substreams, where K is the number of spreading codes used in the system for data transmission. The substreams are broken into M groups, where each substream in the group is spread with a spreading code

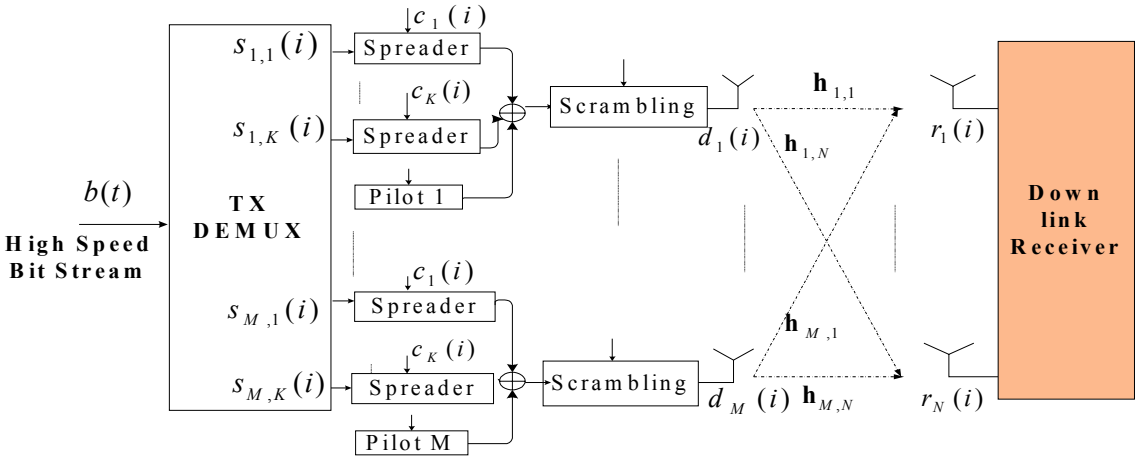

Fig. 1. System model of MIMO Multi-Code CDMA downlink.

of spreading gain G. The groups of substreams are then combined and scrambled with long scrambling codes and transmitted through the m^{th} Tx antenna. The chip level signal at the m^{th} transmit antenna is given by

$$d_m(i) = \sum_{k=1}^{K} s_m^k(j).c_m^k[i] + s_m^P(j).c_m^P[i] \qquad (1)$$

where j is the symbol index, i is chip index and k is the index of the composite spreading code. $s_m^k[j]$is the j^{th} symbol of the k^{th} code at the m^{th} substream. In the following, we focus on the j^{th} symbol and omit the index for simplicity. $c_m^k[i]$= $c^k[i]c_m^{(s)}[i]$ is the composite spreading code sequence for the k^{th} code at the m^{th} substream where $c^k[i]$ is the user specific Hadamard spreading code and $c_m^{(s)}[i]$ is the antenna specific scrambling long code. $s_m^P[j]$ denotes the pilot symbols at the m^{th} antenna. $c_m^P[i]$= $c^P[i]c_m^{(s)}[i]$ is the composite spreading code for pilot symbols at the m^{th} antenna. The received chip level signal at the n^{th} Rx antenna is given by

$$r_n(i) = \sum_{m=1}^{M} \sum_{l=0}^{L_{m,n}} h_{m,n}(l) d_m(i-\tau_l) + z(i) \qquad (2)$$

where the channel is characterized by a channel matrix with elements taken from the channel coefficients between the m^{th} Tx antenna and the n^{th} Rx antenna as

$$h_{m,n}(t) = \sum_{l=0}^{L_{m,n}} h_{m,n}(l)\delta(t-\tau_{m,n,l}). \qquad (3)$$

By packing the received chips from all the receive antennas in a vector $\mathbf{r}(i)=[r_1(i),...,r_n(i),...,r_N(i)]^T$ and collecting the $L_F=2F+1$ consecutive chips with center at the i^{th} chip from all the N Rx antennas, we form a signal matrix as $\overline{\mathbf{r}_A}[i]=[\mathbf{r}(i+F)^T,\ldots,\mathbf{r}(i)^T,\ldots,\mathbf{r}(i-F)^T]^T$. In the vector form, the received signal is given by,

$$\overline{\mathbf{r}_A}[i] = \sum_{m=1}^{M} \mathbf{H}_m \mathbf{d}_m(i), \qquad (4)$$

where

$$\mathbf{H}_m = \begin{bmatrix} \mathbf{h_m}(0) & \cdots & \mathbf{h_m}(L) & & 0 \\ \mathbf{0} & \mathbf{h_m}(0) & \cdots & \mathbf{h_m}(L) & \\ & & \vdots & & \\ & & \vdots & & \\ \mathbf{0} & & \mathbf{h_m}(0) & & \mathbf{h_m}(L) \end{bmatrix}$$

and the multiple receive antennas' channel vector is defined as $\mathbf{h}_m(l)=[h_{m,1}(l),\ldots, h_{m,n}(l),,\ldots, h_{m,N}(l)]^T$. The transmitted chip vector for the mth transmit antenna is given by $\mathbf{d}_m(i)=[d_m(i+F),\ldots, d_m(i),\ldots, d_m(i-F-L)]^T$. The usage of multiple Tx antennas increases the spectrum efficiency dramatically. The achievable data rate increases almost linearly with the number of Tx antennas. For a fully loaded system ($M+K=G$), a pilot is assigned for each Tx antenna. Thus the achievable bit rate is determined by the Tx antenna configuration, the modulation scheme and the chip rate. Table I gives the achievable aggregate uncoded data rate for different number of transmit antennas with a spreading factor (SF) of G=16 and chip rate of 3.84 MHz.

TABLE I. ACHIVEABLE UNCODED DATA RATE

M	K	QPSK(Mbps)	16QAM(Mbps)
1	15	7.2	14.4
2	14	13.44	26.88
4	12	23.04	46.08

III. LMMSE-MIMO EQUALIZER

A. LMMSE Chip Equalizer

Chip level equalization has been one of the most promising receiver algorithms in the single-user CDMA downlink. The chip equalizer estimates the transmitted chip samples by a set of linear FIR filter coefficients as

$$\hat{\mathbf{d}}_m(i) = \hat{\mathbf{w}}_m^H \overline{\mathbf{r}_A}[i]. \qquad (5)$$

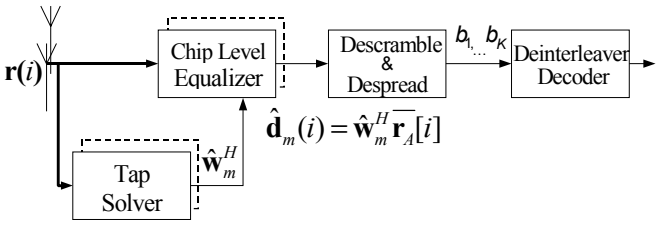

Fig.2. The block diagram of LMMSE equalizer.

Current research consists of two major flavors of equalization, i.e., non-adaptive linear equalizers and adaptive linear equalizers. Non-adaptive linear equalizers usually assume stationarity of the channel in an observation window and design the equalizer with criteria such as LMMSE or zero forcing. It is well known that the LMMSE solution is given by:

$$\begin{aligned}\hat{\mathbf{w}}_m^{opt} &= \arg\min \mathrm{E}[\left\|\mathbf{d_m(i)} - \hat{\mathbf{w}}_m^H \overline{\mathbf{r_A}}[i]\right\|^2] \\ &= \sigma_d^2(i)\mathbf{R}_{rr}(i)^{-1}\mathrm{E}[\overline{\mathbf{r_A}}[i]\mathbf{d}_m^H(i)]\end{aligned} \quad (6)$$

where the correlation matrix is given by the time-average with ergodicity assumption as

$$\mathbf{R}_{rr} = \mathrm{E}[\overline{\mathbf{r}_A}(i)\overline{\mathbf{r}}_{\mathrm{A}}^{\mathbf{H}}(i)] = \frac{1}{N}\sum_{i=0}^{N-1}\overline{\mathbf{r}_A}(i)\overline{\mathbf{r}}_{\mathrm{A}}^{\mathbf{H}}(i) \quad (7)$$

and the channel coefficients are estimated as

$$\hat{\mathbf{h}}_m = \mathrm{E}[\overline{\mathbf{r}_A}[i]\mathbf{d}_m^H(i)] \quad (8)$$

using the pilot symbols. In the HSDPA standard, about 10% of the total transmit power is dedicated to the Common Pilot Channel (CPICH). This will provide accurate channel estimation.

B. Conjugate Gradient Equalizer

To facilitate the comparison and analysis, we give a brief summary of the algorithm in [6] as follows. For the m^{th} transmit antenna, there are two steps involved with a total of J iterations:

1) *Initialization*

$$\mathbf{w}_{m,0} = \mathbf{0}$$
$$\boldsymbol{\gamma}_0 = \mathbf{h}_m; \quad \boldsymbol{\Delta}_0 = \mathbf{h}_m$$
$$\delta_0 = \boldsymbol{\gamma}_0^H \boldsymbol{\gamma}_0; \quad \delta_1 = \delta_0$$

2) *Iteration: for j=1:J*

$$\boldsymbol{\Gamma}_j = \mathbf{R}_{rr}\boldsymbol{\Delta}_{j-1}; \qquad \delta_{j+1} = \boldsymbol{\Gamma}_j^H \boldsymbol{\Gamma}_j$$
$$\alpha = \delta_j / \boldsymbol{\Delta}_{j-1}^H \boldsymbol{\Gamma}_j; \quad \beta = \delta_{j+1}/\delta_j$$
$$\mathbf{w}_{m,j} = \mathbf{w}_{m,j-1} + \alpha\boldsymbol{\Delta}_{j-1}$$
$$\boldsymbol{\gamma}_j = \boldsymbol{\gamma}_{j-1} - \alpha\boldsymbol{\Gamma}_j$$
$$\boldsymbol{\Delta}_j = \boldsymbol{\Gamma}_j + \beta\boldsymbol{\Delta}_{j-1}$$

where $\boldsymbol{\gamma}_j$, $\boldsymbol{\Delta}_j$ are the feed-forward and feedback vector respectively. $\boldsymbol{\Gamma}_j$ is the output vector of the matrix-vector product $\mathbf{R}_{\text{rr}}\boldsymbol{\Delta}_{j-1}$. δ_j, α and β are scalars for fine adjustment at the j^{th} iteration.

C. Frequency-domain Circulant Solution

For a SISO system, it could be shown that a circulant matrix **S** can be diagonalized by the DFT matrix as $\mathbf{S}=\mathbf{D}^{\mathrm{H}}\boldsymbol{\Lambda}\mathbf{D}$, where **D** is the DFT matrix. An extension for the SIMO system has also been derived in [8] utilizing the properties of the Kronecker product. Using the stationarity of the channel and the convolution property, it is easy to show that the correlation matrix is a banded block Toeplitz matrix as

$$\mathbf{R}_{rr} = \begin{bmatrix} \mathbf{E}[0] & \cdots & \mathbf{E}^H[\mathrm{L}] & 0 \\ \vdots & \ddots & \ddots & \\ \mathbf{E}[\mathrm{L}] & \ddots & \ddots & \mathbf{E}^H[\mathrm{L}] \\ & \ddots & & \vdots \\ 0 & & \mathbf{E}[\mathrm{L}] & \mathbf{E}[0] \end{bmatrix}.$$

It can be approximated by a block-circulant matrix after we add two corner matrices as

$$\mathbf{C}_{rr} = \mathbf{R}_{rr} + \begin{bmatrix} \mathbf{0} & \mathbf{0} & \mathbf{C}_L^H \\ \mathbf{0} & \ddots & \mathbf{0} \\ \mathbf{C}_L & \mathbf{0} & \mathbf{0} \end{bmatrix}, \quad (9)$$

where $\mathbf{C}_L = \begin{bmatrix} \mathbf{E}^H[L] & 0 & \\ \vdots & \ddots & \\ \mathbf{E}^H[1] & & \mathbf{E}^H[L] \end{bmatrix}$.

Using the extension of the diagonalization theorem, the block-circulant matrix can be decomposed as

$$\mathbf{C}_{rr} = (\mathbf{D}^H \otimes \mathbf{I})(\sum_{i=0}^{L_F-1}\mathbf{W}^i \otimes \mathbf{E}[i])(\mathbf{D}^H \otimes \mathbf{I}), \quad (10)$$

where $\mathbf{W} = diag(1, W_{L_F}^{-1}, \ldots, W_{L_F}^{-(L_F-1)})$, and $W_{L_F} = e^{j(2\pi/L_F)}$ is the phase factor coefficient for the DFT computation. $\otimes$ denotes the Kronecker product and **D** is the DFT matrix. For an MIMO system, it can be shown that the MIMO equalizer taps are computed as following,

$$\hat{\mathbf{w}}_m^{opt} \approx (\mathbf{D}^H \otimes \mathbf{I}) \cdot \mathbf{F}^{-1} \cdot (\mathbf{D} \otimes \mathbf{I})\hat{\mathbf{h}}_m. \quad (11)$$

$\mathbf{F}=\mathrm{diag}(\mathbf{F}_0, \mathbf{F}_1, \ldots, \mathbf{F}_{\mathrm{LF}})$ is a block-diagonal matrix with elements taken from the element-wise FFT of the first column of a circular matrix. For an $M\times N$ MIMO system, this reduces the inverse of a $(NL_F \times NL_F)$ matrix to the inverse of sub-block matrices with size $N\times N$. For a more complete analysis, we interpret the equation (11) as the following procedure:

(c.1). Compute the independent correlation elements $[\mathbf{E}[0],\ldots,\mathbf{E}[\mathrm{L}]]$, where each element is $N\times N$ sub matrix, and form the first block column of circulant version of $\mathbf{C}_{\text{rr}}$ by adding the corner elements to the end of it as $\mathbf{C}_{rr}^{(1)} = [\mathbf{E}[0],\ldots,\mathbf{E}[\mathrm{L}],0,\ldots,0,\mathbf{E}^{\mathrm{H}}[\mathrm{L}],\ldots,\mathbf{E}^{\mathrm{H}}[1]]^{\mathrm{T}}$.

(c.2). Take the element-wise FFT of $\mathbf{C}_{rr}^{(1)}$ element vectors,

$$\mathbf{F}_{n1,n2} = \mathrm{FFT}\{\mathbf{E}_{n1,n2}^{(c)}\},$$

where $\mathbf{E}^{(c)}_{n1,n2}[i] = \mathbf{C}^{(1)}_{rr}[(n_1\text{-}i\text{-}1)*N+n_2\text{-}1]$, for $i = [0, L_F]$ and n_1, $n_2 \in [1,N]$.

(c.3). For m=[1,M], compute the dimension-wise FFT of the channel estimation as,

$$\mathbf{\Phi}_m = (\mathbf{D} \otimes \mathbf{I})\hat{\mathbf{h}}_m = \mathbf{FFT}([0,...,0,h_{m,n}(L),...,h_{m,n}(0),0,...,0]_{n \in [1,N]}.$$

(c.4). Compute the inverse of the $N \times N$ sub matrix $\mathbf{F}$[i], where

$$\mathbf{F}[i]^{-1} = \left[\mathbf{F}_{n1,n2}[i]\right]^{-1}_{N \times N} = diag(\mathbf{F}[0]^{-1}, \cdots, \mathbf{F}[L_F - 1]^{-1}).$$

(c.5). Compute the matrix multiplication of the inverse of sub-matrices and the FFT output of channel estimation coefficients

$$\mathbf{\Psi}_m = \mathbf{F}^{-1}\mathbf{\Phi}_m.$$

(c.6). Compute the dimension-wise IFFT of the matrix multiplication results, and generate the equalizer taps as

$$\hat{\mathbf{w}}_m^{opt} \approx (\mathbf{D}^H \otimes \mathbf{I})\mathbf{\Psi}_m.$$

IV. Complexity Optimization

A. Hermitian Optimization

For QPSK and QAM modulation, all the numerical computations in this algorithm are associated with complex numbers. However, the complexity in the hardware is reflected by the number of real multiplications, additions, divisions, etc. Because the same operations on different complex numbers will require different hardware resources, it is more accurate to clarify the complexity for different types of computations. For example, a general "Complex (a) × Complex (b)" numerical computation typically has 4 real multiplications and 2 real additions, but a "Complex (a) × Conjugate (a)" reduces to a computation with only 2 real multiplications and 1 real addition. For the Rx antennas n_1, n_2, it can be shown that the elements in the circulant column have the following relations,

$$\begin{cases} \mathbf{E}^{(c)}_{n1,n2}(0) = [\mathbf{E}^{(c)}_{n2,n1}(0)]^* = \sum_{i=0}^{N-1} r_{n1}(i) r_{n2}(i)^*, \\ \mathbf{E}^{(c)}_{n1,n2}(l) = [\mathbf{E}^{(c)}_{n2,n1}(L_F - l)]^* = \sum_{i=0}^{N-1} r_{n1}(i) r_{n2}(i+l)^*, \\ \quad i \in [1, L] \\ \mathbf{E}^{(c)}_{n1,n2}(L_F - l) = [\mathbf{E}^{(c)}_{n2,n1}(l)]^* = \sum_{i=0}^{N-1} r_{n2}(i) r_{n1}(i+l)^*, \\ \quad i \in [1, L] \\ \mathbf{E}^{(c)}_{n1,n2}(l) = \mathbf{E}^{(c)}_{n2,n1}(L_F - l)^* = 0 \quad o.w. \end{cases}$$

Using the features of the FFT, it can be proven that the element-wise FFT results have the relation that $\mathbf{F}_{n1,n2} = [\mathbf{F}_{n1,n2}]^*$. The submatrix formed by the i^{th} entry of $\mathbf{F}_{n1,n2}$ is a $N \times N$ Hermitian symmetric matrix as

$$\mathbf{F}[i] = \left[\mathbf{F}_{n1,n2}[i]\right]_{N \times N} = \mathbf{F}[i]^H. \quad (12)$$

This feature can be used to reduce the complexity dramatically. Instead of having $N \times N$ complex FFT computations, we only need to compute the element-wise FFT for the lower triangular matrix. The number of FFTs in the element-wise FFT is reduced from N^2 to $(N^2+N)/2$. Moreover, the element-wise FFT coefficients of the diagonal elements are all real numbers. This leads to the design of reduced-state MIMO FFT blocks.

B. Reduced-State MIMO-FFT

Because the FFT algorithm applies the features of the rotation coefficients, the application of the *Hermitian* feature in (12) is not straightforward. Here we begin with the standard Decimation-In-Time (DIT) FFT algorithm and derive the hardware-oriented optimization for the reduced-state FFT with pruning operations. Notice that in the standard butterfly unit, each operation involves a full complex multiplication, which has 4 real multiplications and 2 real additions. From (12) we know that

$$f_{m,m}[k] = e_{m,m}[0] + 2\,\mathrm{Re}\left(\sum_{i=1}^{L} e_{m,m}[i] W_{L_F}^{-ki}\right). \quad (13)$$

By defining the input sequence to the FFT module as $\{x(i)\}$ = [0, $e_{m,m}(1)$,…, $e_{m,m}(L)$, 0,…,0], we only need to compute the real part FFT of the $x(i)$ to get $f_{mm}(k)$. From the butterfly decomposition, we have the recursion for the real-part FFT computation as,

$$\begin{aligned} \mathrm{Re}\{X(k)\} &= \mathrm{Re}\{X_1(k)\} + \mathrm{Re}\{W_N^k X_2(k)\} \\ \mathrm{Re}\{X(k+N/2)\} &= \mathrm{Re}\{X_1(k)\} - \mathrm{Re}\{W_N^k X_2(k)\} \end{aligned} \quad (14)$$

for $n = 0,1,...,N/2\text{-}1$. This reduces the complex multiplication and addition to only real multiplication and addition for one stage. The butterfly unit becomes a reduced-state Partial-Butterfly-Unit (PBFU) as shown in Fig. 3 (a).

From the recursion, it can be shown that we can prune the redundant computation by replacing the complex multiplication in the butterfly unit for some portion of the FFT BFU tree. Without considering the feature of the input coefficients that have many zero values, the total number of PBFU is $N\text{-}1$. Since the total number of BFU is $(N / 2)\ \log_2 N$, the total number of Full-BFU (FBFU) is given by $(N / 2)\ \log_2 N - N + 1$.

Consider the fact that $x(n) \neq 0$, n=[1,L], $L < N/2$, we can further truncate computations related to zero values. After pruning all the un-necessary BFU branches, the FBFUs and PBFUs only take effects from stage 3. The number of FBFU is reduced to $(N/2)\ \log_2 N - 2N + 6$. This also reduces the number of memory access and required register files for stage 1 and stage 2 as well as in the partial BFUs. The final data flow is shown as the BFU tree in Fig. 3(b). Only the shaded portion has full BFUs.

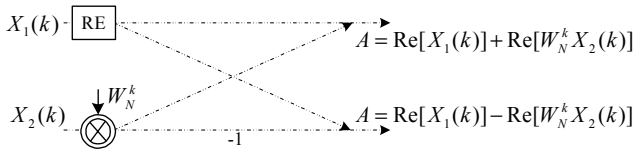

Fig. 3(a). The Partial Butterfly Unit (PBFU) to compute only the real part of the BFU's output.

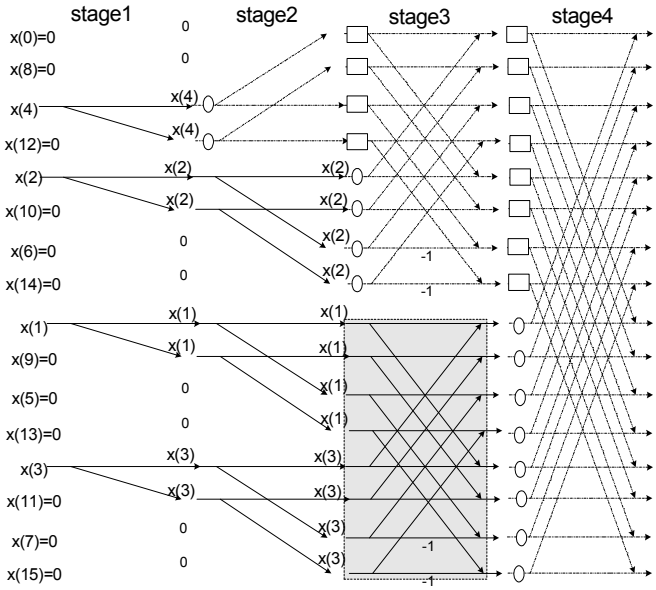

Fig. 3(b). The BFU tree in the RS-FFT with zero-pruning.

Table II summarizes the required operations in terms of the real multiplications/additions and memory read/write. RS-FFT refers to the Reduced-State FFT. ZP indicates Zero-Pruning. Although the savings diminish when the length of FFT increases to a very large number, for the equalizer application, the length of the FFT remains in the range of 64-point FFT. The RS-FFT with ZP saves roughly 50% of the real multiplications. This is shown in Fig. 4 for 16, 32 and 64-point FFTs. So the equivalent number of element-wise FFTs is reduced to $N^2/2$.

The *Hermitian* feature of the element-wise FFT also leads to reduced complexity in the $N \times N$ submatrix inverse and facilitates the succeeding computation with the dimension-wise FFT of the channel coefficients. The saving is also roughly 50%. Because of the limited space here, the detailed description of the hardware architecture will be presented in a future paper.

V. Performance & Complexity

A. BER Performance

The performance is evaluated in an HSDPA simulation chain for different MIMO antenna configurations. We compare the performance of four different schemes: the Direct-Matrix-Inverse (DMI), the Conjugate-Gradient (CG) algorithm, the FFT-based algorithm and the LMS adaptive algorithm. We simulated the Pedestrian-A and Pedestrian-B channels following the I-METRA channel model [9][10]. The chip rate for the transmit signal is 3.84 Mcps, which is in compliance with the 3GPP HSDPA standard. Orthogonal-Variable-Spreading-Factor (OVSF) codes are generated from the Hadamard sequence. The spreading gain is G and the number of spreading codes is K for the data channel. Notice that unlike the conventional CDMA downlink, in a Multi-Code CDMA system such as HSDPA, all the K codes are assigned to one single user to achieve high data rate downlink service. The channel state information is estimated from the CPICH at the receiver. 10% of the total transmit power is dedicated to the pilot training symbols.

TABLE II. Complexity Comparison For Different FFT Schemes

	Real Mult	Real Add
Full FFT	$2N\log_2 N$	$N\log_2 N$
RS-FFT w/o ZP	$2N\log_2 N-2N+2$	$N\log_2 N-2N+2$
RS-FFT with ZP	$2N\log_2 N-6N+12$	$N\log_2 N-4N+12$

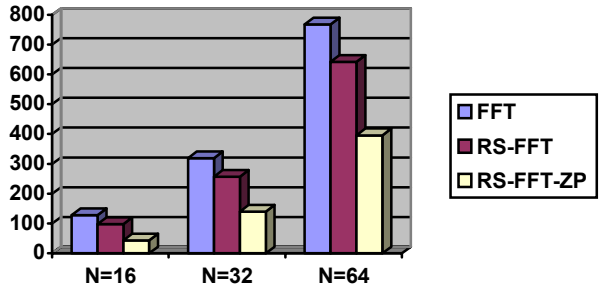

Fig. 4. The number of real multiplications in RS-FFT.

We provide the simulation results for different MIMO antenna configurations in the form of ($M \times N$) with the QPSK modulation scheme. In the figures, L_h is shown as the channel delay spread. Fig. 5 shows the 1×2 case under Pedestrian-A for a fully loaded system. Fig. 6 and Fig. 7 show the fully loaded system for Pedestrian-A and Pedestrian-B channels with 2×2 configuration, while Fig. 8 shows a highly loaded system with 10 codes for 2×2 Pedestrian-B channel. Fig. 9 shows the simulation results for Pedestrian-A with 4×4 configuration. It can be seen from Fig. 5 and Fig. 6 that the FFT-based algorithm overlaps with both the DMI and the CG at 5 iterations very closely. In a 2×2 case for Pedestrian-B channel, both the CG and the FFT-based algorithm shows very small divergence from the DMI at the very high SNR range in Fig. 7 and Fig. 8. For a fully loaded system, CG with 5 iterations seems to be slightly better than the FFT-based algorithm. But in a case with 10 codes, the FFT-based algorithm outperforms the CG for both 3 iterations and 5 iterations. In the 4×4 case as shown in Fig. 9, the FFT-based algorithm also outperforms the CG with 5 iterations. However, considering the fact that the physical system is most unlikely to work in a very high SNR range, the small difference in the BER performance is negligible. In all cases, the DMI, CG and FFT-based algorithms significantly outperform the LMS adaptive algorithm. Higher-order modulation schemes such the 16-QAM and the 64-QAM are common practice for HSDPA. We have extensive simulation results showing similar results for the proposed algorithm compared with the exact LMMSE

algorithm. Because of the limited space in this paper, we omit the higher-order modulation results here.

B. Complexity

Since hardware complexity is a very important consideration, we also compare the complexity of three schemes with similar performance, i.e., the DMI, the CG and the FFT-based algorithm. Cholesky decomposition is applied in the DMI computation. The complexity is compared in terms of the number of equivalent complex multiplications and additions. Although the complete equalizer system consists of the correlation matrix computation as the initialization part with the tap solver and the FIR filtering as the data processing part, we focus on the tap solver part for comparison because the other two computations are common for the algorithms presented here. For the DMI, the complexity is of the order of $O\{[N(F+1)]^3\}$ for the matrix inverse of $\mathbf{R}_{rr}$ and $O\{[N(F+1)]^2M\}$ for the matrix multiplication of $(\mathbf{R}_{rr})^{-1}\mathbf{h}_m$. For the CG, there are $O\{MJ[N(F+1)]^2 + M(5J+1)N(F+1)\}$ complex multiplications and $O\{MJ[N(F+1)]^2 + 8MJN(F+1)\}$ complex additions. For the FFT-based algorithm, the overall complexity before *Hermitian* optimization is $O\{(N^2+2MN)L_F(\log_2 L_F)/2+(N^3+MN^2)L_F\}$. With the *Hermitian* optimization, the complexity reduces to $O\{(N^2/2+2MN)L_F(\log_2 L_F)/2+(N^3+MN^2)L_F/2\}$.

Usually, $J = 5$ iterations for the CG algorithm will suffice for convergence near the DMI solution. For the FFT-based algorithm, we usually require $L_F \geq 2F+1$. The complexity is summarized in Table III. For simplicity, we only list the most significant part of equivalent number of complex multiplications. An example is given for the 4×4 case with $F = 10$, $J = 5$. The length of FFT $L_F = 32$ will suffice for both Pedestrian A and Pedestrian B channels. In Fig. 10, we show the complexity comparison for different J and different L_F vs. the different channel lengths for a 4×4 antenna configuration. To apply the benefit of FFT, the length of FFT is chosen to be the power of 2. This results in the staircase complexity in Fig. 10. It is clear that the Conjugate Gradient algorithm has reduced complexity compared with the DMI, while the complexity reduction for the FFT-based algorithm is the most significant.

VI. Conclusion

In this paper, we proposed an FFT-based MIMO chip equalizer with reduced complexity for Multi-Code CDMA downlink. A comparative study is presented between the DMI, CG and FFT-based equalizers in terms of both performance and complexity. It is demonstrated that the proposed algorithm has much lower computational complexity while maintaining the performance. This will significantly facilitate the hardware implementation in the mobile device.

Acknowledgements

We are grateful to Predrag B. Radosavljevic for his simulation environment and Dr. Behnaam Aazhang for his helpful comments. J. R. Cavallaro was supported in part by NSF under grants ANI-9979465, EIA-0224458 and EIA-0321266.

References

[1] Y. Guo, J. Zhang, D. McCain, J. R. Cavallaro, "Scalable FPGA Architectures for LMMSE-based SIMO Chip Equalizer in HSDPA Downlink", *37th IEEE Asilomar Conference on Signals, Systems and Computers*, 2003.

[2] A. Wiesel, L. García, J. Vidal, A. Pagès, Javier R. Fonollosa, "Turbo linear dispersion space time coding for MIMO HSDPA systems", 12th IST Summit on Mobile and Wireless Communications, June 15-18, 2003, Aveiro, Portugal.

[3] G. J. Foschini, "Layered space–time architecture for wireless communication in a fading environment when using multielement antennas", *Bell Labs Tech. J.*, pp. 41–59, 1996.

[4] G. D. Golden, J. G. Foschini, R. A. Valenzuela, and P. W. Wolniansky, "Detection algorithm and initial laboratory results using V-BLAST space-time communication architecture," *Electron. Lett.*, vol. 35, pp.14–15, Jan. 1999.

[5] K. Hooli, M. Juntti, M. J. Heikkila, P. Komulainen, M. Latva-aho, J. Lilleberg, "Chip-level channel equalization in WCDMA downlink", *EURASIP Journal on Applied Signal Processing*, Aug.2002, pp. 757-770.

[6] M. J. Heikkila, K. Ruotsalainen and J. Lilleberg, "Space-time equalization using conjugate-gradient algorithm in WCDMA downlink ", IEEE Proceeding in PIMRC, pp. 673-677, 2002.

[7] P. Radosavljevic, J. R. Cavallaro, A. D. Baynast, "ASIP architecture implementation of channel equalization algorithms for MIMO systems in WCDMA downlink", IEEE Vehicular Technology Conference (VTC), Los Angeles, CA, Sept. 2004.

[8] J. Zhang, T. Bhatt, G. Mandyam, "Efficient linear equalization for high data rate downlink CDMA signaling", 37th *IEEE Asilomar Conference on Signals, Systems and Computers*, 2003.

[9] J.P. Kermoal, L. Schumacher, K. Pedersen and P. Mogensen, "A Stochastic MIMO Radio Channel Model with Experimental Validation", *IEEE JSAC*, VOL. 20, NO. 6, Aug. 2002, pp.1211-1226.

[10] I-METRA project consortium, "The IST-2000-30148 I-METRA project," in http://www.ist-imetra.org.

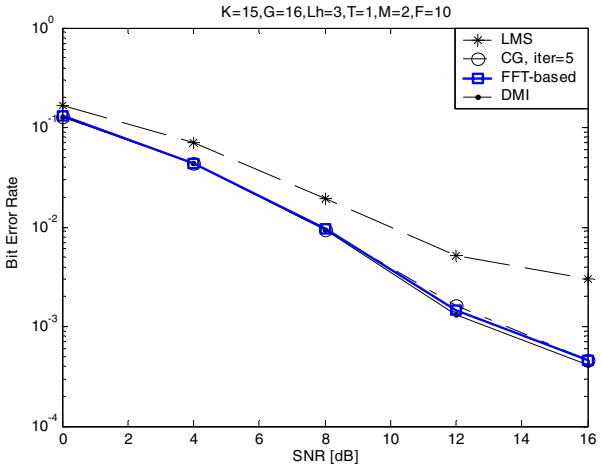

Fig. 5. Bit-Error-Rate for fully loaded Pedestrian-A channel with antenna configuration of 1×2.

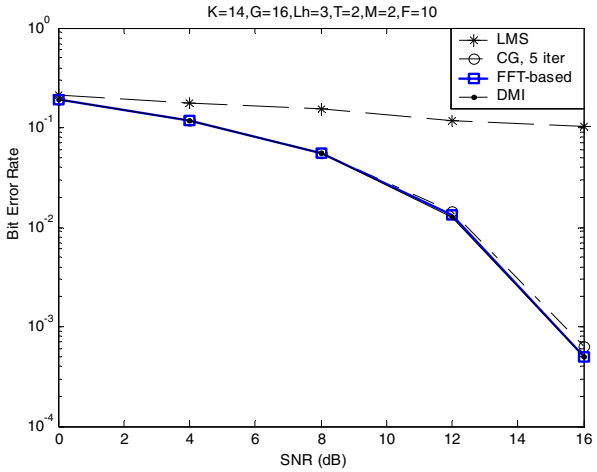

Fig. 6. Bit-Error-Rate for fully loaded Pedestrian-A channel with antenna configuration of 2×2.

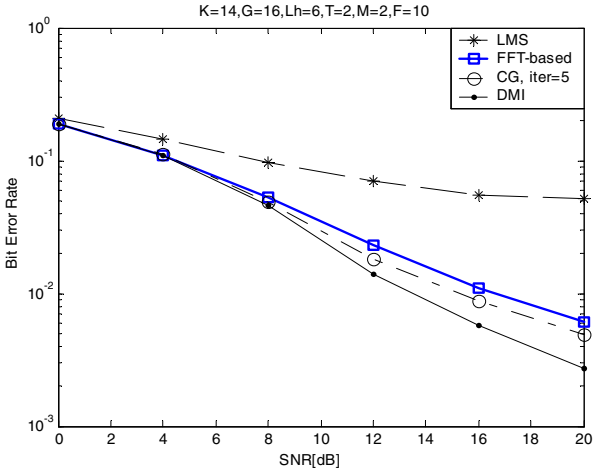

Fig. 7. Bit-Error-Rate for fully loaded Pedestrian-B channel with antenna configuration of 2×2.

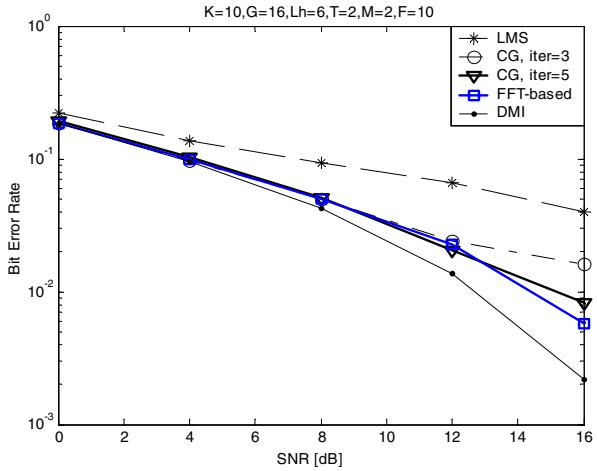

Fig. 8. Bit-Error-Rate for highly loaded Pedestrian-B channel with antenna configuration of 2×2.

TABLE III. ALGORITHM COMPLEXITY COMPARISON

	Equivalent Complex Multiplication	Example
DMI	$O\{(M+NF)(NF)^2\}$	92928
CG	$O\{JM[(NF)^2+5NF]\}$	43120
FFT-based	$O\{(N^2/2+2MN)(\log_2 L_F)+(N^3+MN^2)\}L_F/2\}$	5248

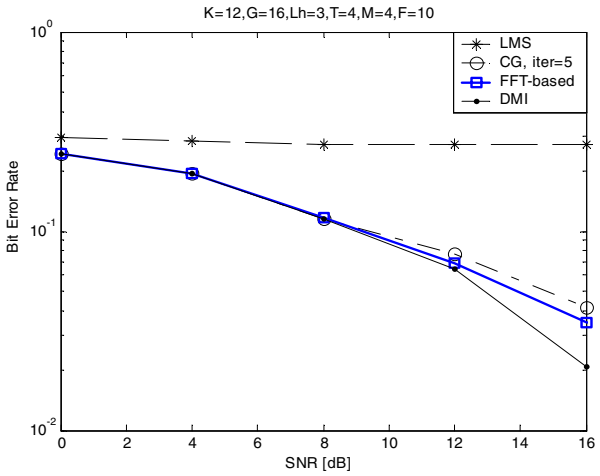

Fig. 9. Bit-Error-Rate for fully loaded Pedestrian-A channel with antenna configuration of 4×4.

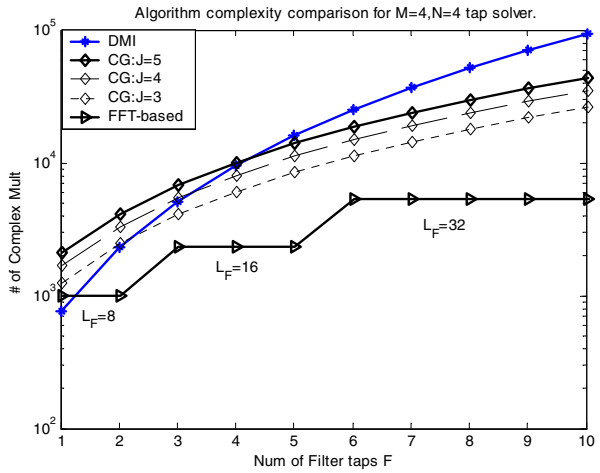

Fig. 10. The complexity comparison for 4×4 tap solver.